

School of Physics and Astronomy



Energy-efficient device platforms based on vdW magnets

First Year Report and Literature Review

Shreyas Ramachandran
October 2024

Abstract

The recent push towards energy-efficient devices has led to a special focus on layered antiferromagnetic materials such as MnPS₃. MnPS₃ is known to have rich domain wall dynamics and has previously been used for magnon transport. This study uses atomistic simulations to probe the domain wall dynamics of 1-7 layered MnPS₃ flakes for an array of magnetic fields. Domain wall motion is observed for odd-layered flakes at all fields whereas even-layered flakes have pinned domain walls up to the spin-flop transition. Both odd and even layers show spin wave emissions in the spin-flop regime. A saturation of domain wall velocities beyond the spin-flop transition is observed for odd-layered flakes. The thickness dependence of domain wall velocities in the spin-flop regime is analysed and is found to be 450 m/s at 100 nm thickness. This study provides insights into the fundamental processes involved in anti-ferromagnetic transitions and how thickness can be used to tune domain wall motion.

Signature:

Supervisor: Dr. Elton Santos

Date: 9 October 2024

Contents

1	Introduction	2
1.1	Background	2
1.2	Early Progress in 2D Magnets	3
1.3	2D Anti-Ferromagnetic Materials and Spintronics	6
2	Progress to Date	9
2.1	Methods	9
2.2	Results	11
2.2.1	Verification of simulation parameters	11
2.2.2	Domain wall dynamics of odd-layered MnPS ₃	12
2.2.3	Domain wall dynamics of even-layered MnPS ₃	15
3	Future Work	17
4	Summary	17

1 Introduction

1.1 Background

The global push towards sustainability and alternative energy sources has resulted in actions such as the Paris Agreement [1] and the Net Zero Coalition [2]. Now more than ever there is an immense need for development in energy storage and conversion. However, to truly reach the Net Zero goals, research must also focus on the energy efficiency of electronic devices. Moore's papers in 1965 and 1975 [3, 4] boldly predicted that the number of transistors in an integrated chip would double every two years - a statement that has since then been termed a "law". However, traditional devices have reached the limits of their scaling and the search is now on for new architectures, memory devices and even logic gates [5]. Additionally, Lundstrom [6] identified critical limitations to chip development in the early 2000s. He put forth alternatives such as new materials and reducing the dimensionality of devices to overcome problems which included leakage current and heat dissipation.

The use of magnetism in devices has been around for more than 100 years, primarily for information storage and more recently for alternative memory devices such as MRAM and spintronics. From floppy disks in the 1970s to CDs and DVDs in the 1990s and finally hard drives and solid state drives there has been a significant increase in the areal information density. This development has gone hand in hand with our understanding of magnetism and our ability to control the magnetic properties of materials [7]. However, as we develop new energy-efficient architectures and computing methods, we must ensure that our data storage technologies also become increasingly energy-efficient. Recently, spintronic devices have emerged as a possible route for data storage. In these devices, electron spin is used as an additional degree of freedom that can be used to store data [8].

Since the discovery of graphene in 2004 [9], the field of 2D materials has seen extensive research effort over the last two decades. Our improved understanding of their physical and electronic properties has opened the doors for many applications including but not limited to energy storage, sensing and electronic devices [10]. In the context of energy, 2D materials have become key players in various applications such as catalysis, batteries, supercapacitors and hydrogen storage among others [11, 12, 13, 14]. However, the search for lucrative magnetic materials that can be used for next-generation devices has excluded 2D materials for the most part due to Mermin and Wagner's work in which they put forth that long-range magnetic order is suppressed in 2D thin films at finite temperatures in the thermodynamic limit [15]. But this changed in 2017 with the discovery of magnetism at finite temperatures in monolayers of $\text{Cr}_2\text{Ge}_2\text{Te}_6$ [16] and CrI_3 [17] which has elicited a surge in the previously unthinkable 2D magnetism. Several 2D magnetic materials have been discovered since such as Fe_3GeTe_2 , CrCl_3 , Fe_3GaTe_2 , MnPS_3 along with the original CrI_3 and $\text{Cr}_2\text{Ge}_2\text{Te}_6$ that show a variety of magnetic properties suitable for a plethora of applications [18].

2D magnets possess some fundamental properties that make them attractive for future devices. These materials can be tuned using factors such as the number of layers, stacking order, symmetry or even choice of substrates. The electronic properties of these materials are also extremely varied with some 2D magnets showing metallic character while others are insulators. Additionally, these materials interact primarily with weak van der Waals

forces between layers which significantly reduce negative interfacial losses. The field of 2D magnetism is still in its infancy with a lot of new materials being discovered every few months. In this context, theory and simulation play an important role in determining material behaviour from a quantum and atomic level which can guide the discovery and development of new materials. Modelling 2D materials across various length scales allows us to study the interplay between magnetic factors such as anisotropy, the type of magnetic interactions, and magnetic moments and structural factors such as the number of layers, heterostructures, and doping. For example, a recent breakthrough in 2D magnetism used large-scale simulations to invalidate the applicability of the Mermin-Wagner theorem in 2D materials at experimental time- and length-scales [19]. This highlights the capabilities of simulations in understanding the underlying mechanisms that govern the magnetic properties of 2D materials. It is, therefore, crucial to combine experiment and theory to rapidly develop this emerging field of 2D magnets for future devices [18].

1.2 Early Progress in 2D Magnets

Magnetism in 2D materials up to a few-layer limit was first observed in the seminal works by Gong and Huang and their respective coworkers [16, 17]. While previous works utilised thin films to reduce dimensionality in magnetic systems [20], long-range order in the truly 2D limit was still hindered by the Mermin-Wagner theorem [15]. Using a simple Heisenberg model with only first-neighbour isotropic exchange, Mermin and Wagner postulated that long-range order magnetic order in $N < 3$ dimensions is suppressed at finite temperatures due to thermal fluctuations breaking the order. This implied that 2D and 1D systems could not show ferromagnetism or anti-ferromagnetism without additional effects such as anisotropy due to crystal structure or geometry [15].

Indeed, Gong and coworkers showed that external magnetic fields could be used to control the transition temperature in exfoliated $\text{Cr}_2\text{Ge}_2\text{Te}_6$ bilayers [16]. They used magneto-optical Kerr microscopy to observe ferromagnetic order in a bilayer $\text{Cr}_2\text{Ge}_2\text{Te}_6$ flake as they reduced the temperature from 40 K to 4.7 K in the presence of a small magnetic field of 0.075 T. They further proposed that the transition temperature was primarily determined by exchange interactions in 3D whereas anisotropy or external fields could control the transition temperature in 2D layers of $\text{Cr}_2\text{Ge}_2\text{Te}_6$ [16]. Around the same time, Huang and coworkers investigated the magnetic properties of CrI_3 down to the monolayer limit and observed Ising ferromagnetism in monolayers and trilayers [17]. CrI_3 shows a strong out-of-plane anisotropy that allows it to behave as an Ising ferromagnet [21]. They hypothesized that this strong anisotropy allowed CrI_3 to circumvent the Mermin-Wagner theorem and show long-range ferromagnetic order even in the monolayers. Furthermore, they observed an anti-ferromagnetic ordering between layers as the bilayer samples showed vanishing Kerr rotations with external fields between ± 0.65 T. The layer-dependent magnetic properties of CrI_3 could therefore be used to engineer magneto-electronic devices at low temperatures [17].

Following Gong and Huang's works, several experimental realisations of magnetism in 2D materials such as Fe_3GeTe_2 [22], NiPS_3 [23], CrCl_3 [24] were realised. This sparked an interest in the theory and simulation of these materials as a fundamental understanding of the origin of their magnetic properties would only enable further development in the field. Both Gong's and Huang's works proposed external fields and inherent anisotropies as the

main reasons for the finite transition temperature in the 2D limit [16, 17]. However, Jenkins and coworkers performed extremely large-scale atomistic simulations using an isotropic Heisenberg Hamiltonian with only nearest neighbours (similar to Mermin and Wagner's work [15]) up to $1 \mu\text{m} \times 1 \mu\text{m}$ system sizes [19]. They found that short-range magnetic order existed even at experimentally accessible time and length scales due to exchange interactions and factors such as anisotropy, geometry and external fields affected the preferential direction rather than the inherent cause of magnetisation [19]. These results prompted several studies combining experiment and theory to study the feasibility of 2D magnetic materials for next-generation devices [25, 26, 27, 28].

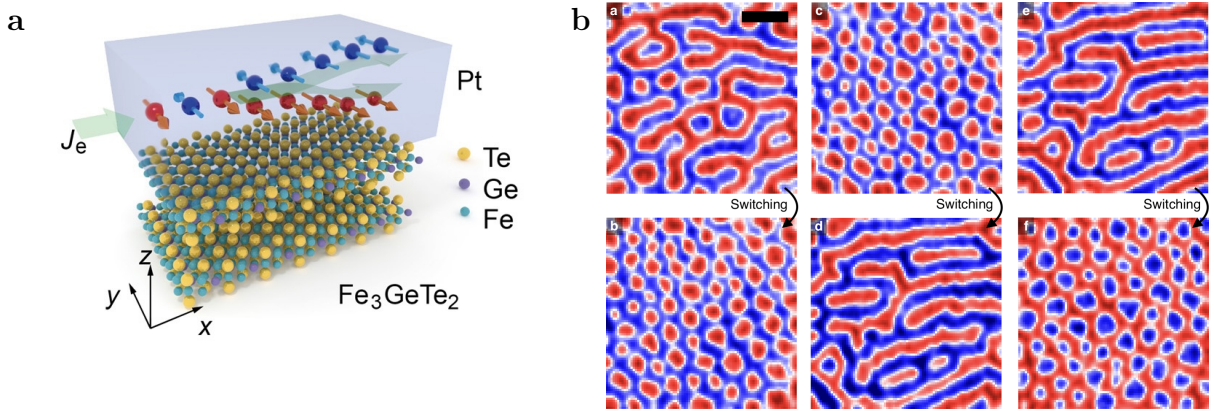


Figure 1: (a) Schematic of device fabricated in Ref. [25]. Green arrow represents in-plane current flowing into Pt layer. The separation of spins creates a spin current in the z direction which exerts a torque on the FGT bilayer below (Adapted from Ref. [25]). (b) Switching mechanism observed in Ref. [26]. $a-b$ is the switching from strip state to the bubble state in the presence of out-of-plane magnetic field. $c-d$ is the switching from the bubble state b to the stripe state with no magnetic field. $e-f$ is the switching from stripe state d to the bubble state of opposite polarity with an out-of-plane field in the reverse direction (Adapted from Ref. [26]).

Magnetisation switching is crucial for applying 2D magnets in spintronic devices, which use spin as an additional degree of freedom in addition to charge states [29]. Wang and coworkers fabricated a layered device with Pt and Fe_3GeTe_2 (Figure 1a) where the magnetisation of ferromagnetic Fe_3GeTe_2 could effectively be switched by passing current through the Pt layer [25]. The strong spin-orbit coupling of Pt results in a spin Hall effect when current passes through it causing a spin current in the perpendicular direction. This spin current exerts a torque on the magnetisation of the Fe_3GeTe_2 layers, known as Spin-Orbit Torque (SOT). The spins in Fe_3GeTe_2 are aligned out-of-plane and Wang et al observed magnetisation switching due to the SOT from the Pt layer when an in-plane magnetic field was applied [25]. On the other hand, Khela and coworkers used ultrafast laser pulses to induce reversible switching of spin textures in CrGeTe_3 [26]. In the presence of a small out-of-plane magnetic field, laser pulses applied to samples of CrGeTe_3 stabilised small magnetic "bubble" domains or magnetic "stripe" domains depending on the number of laser pulses. Furthermore, light pulses without a magnetic field could switch a bubble state to a stripe state. The stripe state could then be switched back to a bubble state using light pulses by applying an out-of-plane magnetic field wherein the polarity determined the magnetisation direction of the bubble domains [26]. The experimental snapshots of the switching process are shown in Figure 1b. Several other

realisations of magnetisation switching in 2D magnetic materials further highlighted the potential of these materials for future devices [30, 31, 32].

Another area of growing interest in 2D magnets with emerging potential in next-generation devices is spin textures such as skyrmions, merons and domain walls [18]. Several experimental and theoretical realisations of topological spin features are already present in the literature [27, 28, 33]. Park and coworkers observed Néel-type skyrmions in Fe_3GeTe_2 based heterostructures and used short current pulses to move a skyrmion along the heterostructure [27]. The Fe_3GeTe_2 heterostructures had oxidised layers at the interfaces which broke the inversion symmetry. This broken symmetry along with the high Spin-Orbit Coupling (SOC) of Fe_3GeTe_2 results in antisymmetric exchange interactions, also known as Dzyaloshinskii-Moriya Interactions (DMI) [27]. DMI favours canting of spins as opposed to exchange interactions that prefer collinear ordering between spins [34, 35]. When the DMI is strong enough, it can stabilise topological spin textures such as skyrmions [36]. Park and coworkers further demonstrated the ability to drive skyrmions in the Fe_3GeTe_2 heterostructure using short current pulses (shown in Figure 2a), which further highlights the applicability of such materials to next-generation devices, such as a racetrack memory device (Figure 2b) [27, 37].

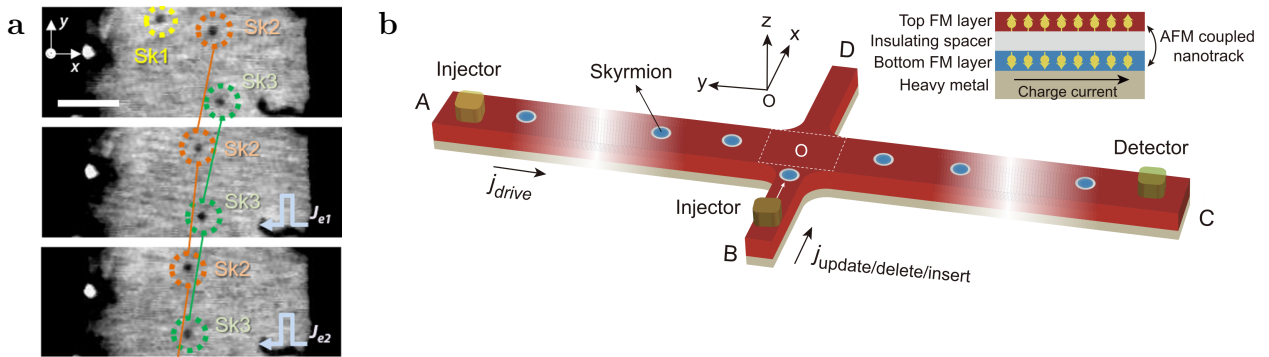


Figure 2: (a) Sequential images of FGT device used in Ref. [27] taken after each current pulse in the $+x$ direction (electron injection in $-x$) showing skyrmion motion. Individual skyrmions and their displacement are highlighted for clarity (Adapted from Ref. [27]). (b) Schematic of a racetrack memory using skyrmions proposed by Zhu et al. in Ref. [37]. Injectors A and B create and modify skyrmions, while C is the detector. The diagram in the top right depicts the layered structure employed in the racetrack (Adapted from Ref. [37]).

In summary, the field of 2D magnets is still in its infancy and has immense potential for applications in energy-efficient devices. Since its inception, magnetism in 2D materials has been the focus of many studies, experimental and theoretical. Initial studies believed that the cause of magnetism in 2D materials were factors related to magnetocrystalline anisotropy, geometry or external fields [16, 17, 22]. However, with the help of theory and simulation, exchange interactions were shown to be the major factor in stabilising magnetic order with the external factors deciding the magnetisation direction [19]. To explore the feasibility of 2D magnets in next-generation devices, several studies successfully fabricated devices with 2D materials. Some studies showed that 2D magnets had robust magnetic switching capabilities in spin states and spin textures [25, 26, 32]. Other works could stabilise topological spin textures such as skyrmions and merons and even control their motion [27, 28]. These results illustrate the capability of 2D magnets for

energy-efficient spintronic applications.

1.3 2D Anti-Ferromagnetic Materials and Spintronics

In the context of energy-efficient devices, antiferromagnetic spintronics is a rapidly growing field which has garnered special interest in recent years [38]. Compared to ferromagnets, anti-ferromagnets have a much higher exchange energy and as such it is harder to orient the magnetisation in anti-ferromagnets with magnetic fields. This means that anti-ferromagnets do not generate stray magnetic fields and also are robust against magnetic field perturbations - thus reducing the possibility of data loss in magnetic storage systems [38]. Additionally, reorientation or canting of magnetic moments in anti-ferromagnets costs exchange energy whereas in the case of ferromagnets, only anisotropy energy is required. As a result, the magnetisation dynamics are much faster in anti-ferromagnets than in ferromagnets [39].

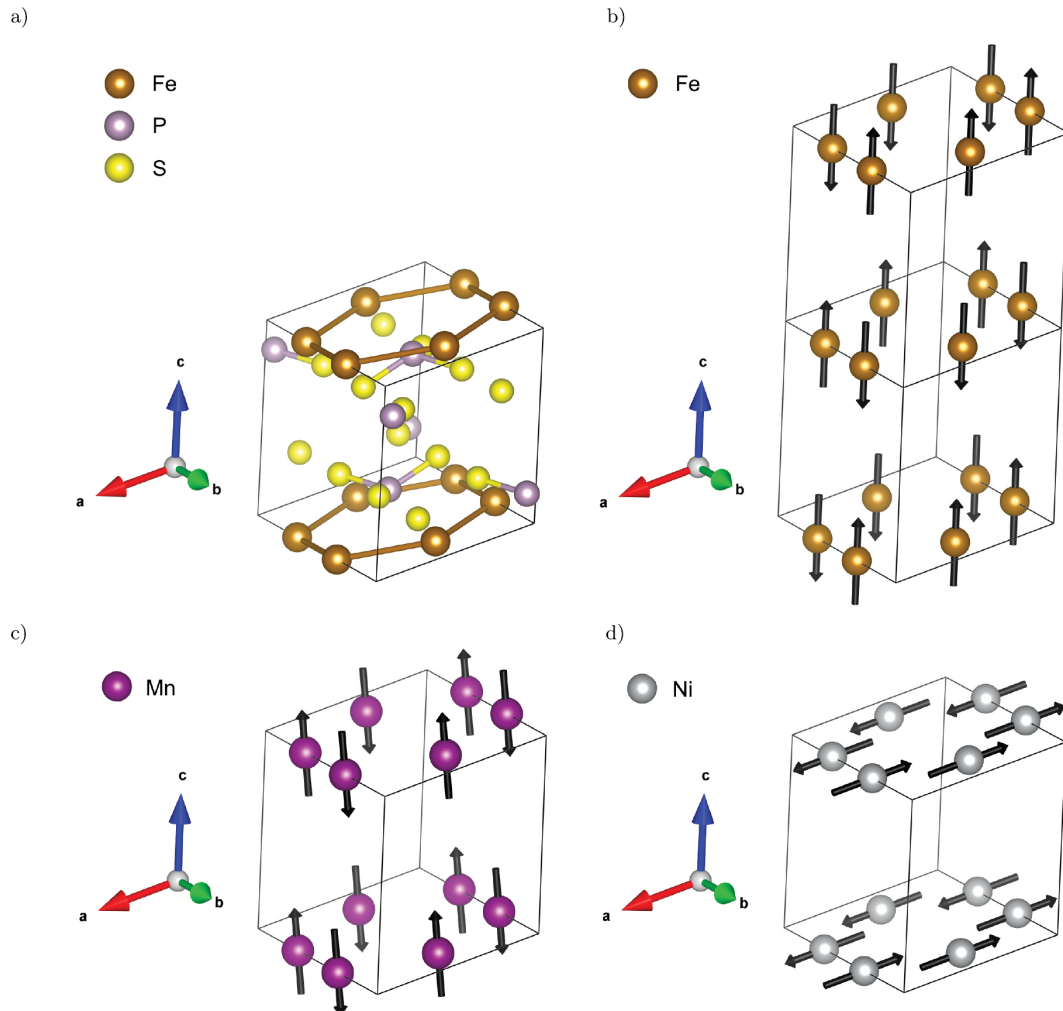


Figure 3: (a) Crystal structure of MPX₃ family using FePS₃ as an example. Fe atoms are in brown, P in lavender and S in yellow. (b) Magnetic structure of FePS₃. (c) Magnetic structure of MnPS₃. Mn atoms are shown in magenta. (d) Magnetic structure of NiPS₃. Ni atoms are shown in grey. P and S atoms are omitted from all magnetic structures. Arrows indicate the direction of spin on the atoms. Adapted from Ref. [40]

Generally, within 2D materials, Anti-ferromagnetic ordering can be of two types - layered and intrinsic. In the layered case, the magnetic ordering is ferromagnetic within the layer with anti-ferromagnetic coupling between the layers, for example, CrCl_3 [24]. The intrinsic case is when the magnetic ordering within and between layers is Anti-ferromagnetic. The Metal Phosphorous Trichalcogenide MPX_3 ($\text{X}=\text{S}, \text{Se}$) family is an example of an intrinsic anti-ferromagnet [41]. The anti-ferromagnetic coupling within the layers is highly desirable as it can stabilise long-range magnon transport [42]. Additionally, the MPX_3 family has an array of magnetic and electronic properties with band gaps varying from 1.3-3.5 eV and Néel temperatures ranging from 78-155 K, making it the focus of significant research in recent times[41].

Within the MPX_3 family, the choice of transition metal affects the magnetic ground state of the material. All MPX_3 compounds have the same crystal structure - a $C2/m$ monoclinic cell with a honeycomb arrangement of metal ions that act as magnetic sites (Figure 3a) [40]. As seen in Figure 3b, FePS_3 has Ising spins oriented along c^* that form chains along a with anti-ferromagnetic coupling between the chains in-plane and out-of-plane. MnPS_3 is best described by the Heisenberg model with the spins canted 8 deg from the c^* axis that are coupled anti-ferromagnetically to their nearest neighbours (in-plane and out-of-plane), shown in Figure 3c. In NiPS_3 , the magnetic spins are oriented along the a vector with neighbouring chains being anti-ferromagnetically coupled in-plane. Additionally, the out-of-plane coupling between the chains is ferromagnetic, as shown in Figure 3d [40]. These differences in the magnetic ordering give rise to a wide variety of magnetic properties in the MPX_3 family, controllable by the choice of transition metal [41, 40].

In particular, MnPS_3 has received a lot of focus in recent times due to its small anisotropy relative to the exchange energy, which is the lowest among the MPX_3 family [43]. Studies have shown that magnon transport over several micrometres is possible in MnPS_3 [42], and it is also possible to control the magnon transmission using a gate current [44]. Furthermore, Chen and coworkers showed a NOT logic gate functionality for a MnPS_3 magnon device with Pt electrodes that was fully reversible [44]. In their work, an injection current generated the spin-wave in MnPS_3 which, after travelling through the device, caused a voltage difference across the detector due to the inverse spin Hall effect. The gate current controls the voltage as the Joule heating from the gate current would reduce the magnon mean-free length and thus disrupt the magnon transport, thus making the voltage fully switchable [44]. These studies firmly establish MnPS_3 as a strong candidate for energy-efficient spintronic and magnonic devices.

Indeed, several theoretical studies probing the magnetic properties of MnPS_3 already exist in literature [45, 46, 47, 48]. Amirabbasi and Rybak and their respective coworkers used first-principles to study the magnetic properties of monolayers of several members of the MPX_3 family. They used Density Functional Theory (DFT) to extract electronic properties such as band gaps and the Density of States (DOS) [47, 48]. Rybak and coworkers focused on magneto-optical properties and were able to observe different transitions for in-plane and out-of-plane ordering of spins in MnPS_3 [48]. Amirabbasi and coworkers parametrized spin Hamiltonians to their DFT calculations and extracted exchange couplings, biquadratic interactions, and anisotropy for MPS_3 ($\text{M}=\text{Mn, Fe, Co, Ni}$). They further observed that MnPS_3 was the only material to have a Néel ground state while the others primarily had anti-ferromagnetic zig-zag chains that were stabilised by strong third neighbour exchange interactions [47].

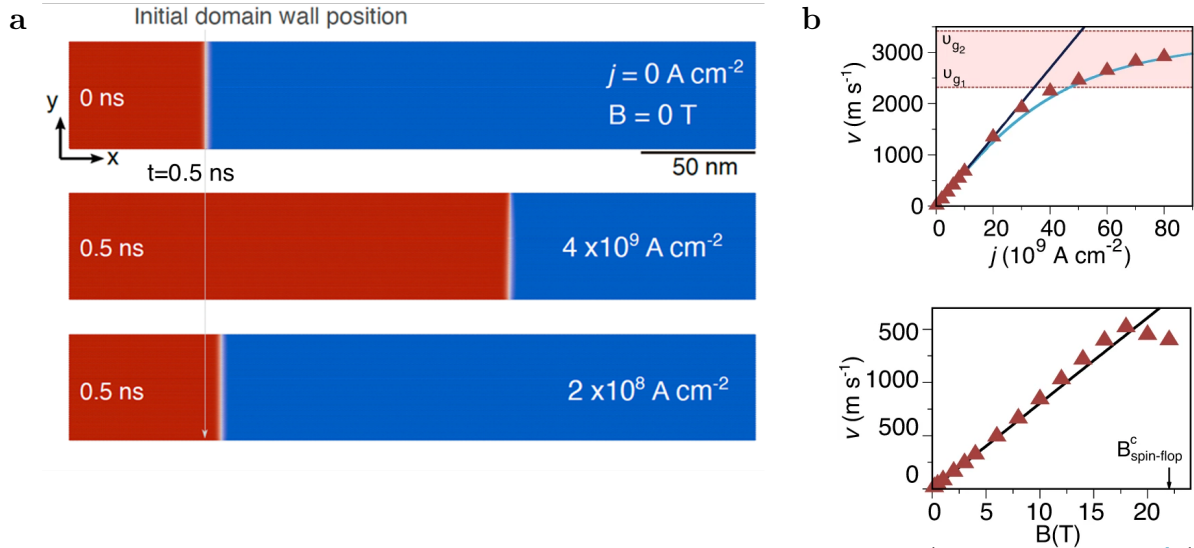


Figure 4: Exchange interactions considered for VAMPIRE simulations of MnPS_3 . (a) In-plane (adapted from Ref [45]) (b) out-of-plane (adapted from Ref [46]).

Alliati and coworkers explored the rich domain wall dynamics of MnPS_3 and were able to move domain walls with electric currents and magnetic fields [45]. The domain wall dynamics approached the relativistic regime at high current densities, reaching maximum speeds of 3000 m s^{-1} at $j = 80 \times 10^9 \text{ A cm}^{-2}$. While using magnetic fields, the domain wall speeds increased with the field till the spin-flop field. Beyond the spin-flop field, the spins align themselves in the ab plane which allows for restructuring of spin textures. Interestingly, when increasing the current densities, the domain wall widths decreased and the domain wall mass increased whereas the opposite trend was observed with magnetic fields. Furthermore, domain wall motion depended on the edge terminations. Along b , the armchair edges resulted in no domain wall motion leading to a "pinned" domain wall. Along a , electric currents could move the wall regardless of a zig-zag or dangling bond edge but magnetic fields could only move the wall with a zig-zag edge on one side and a dangling bond edge on the other [45]. These results suggest that the domain wall dynamics in MnPS_3 is extremely sensitive to, yet controllable by, factors such as external fields.

The sensitivity of domain wall dynamics in MnPS_3 was further observed by a collaborator of the research group, Dr Xiao-Xiao Zhang and her coworkers at the University of Florida, USA. Using extremely sensitive nanoelectromechanical (NEMS) resonators, they could detect changes in resonant frequencies of the order of tens of kHz. While sweeping the applied out-of-plane magnetic field between $\pm 10 \text{ T}$, they observed two transitions at $\pm 4.6 \text{ T}$ and $\pm 7 \text{ T}$ respectively, as shown in Figure 5a. The transition at $\pm 4.6 \text{ T}$ is close to that of experimentally reported values of the spin-flop field [49] whereas the transition at $\pm 7 \text{ T}$ has not yet been identified. At the transition fields, Dr Zhang and her coworkers also find a sharp drop in the quality factor. They postulated that there could be strong dissipation channels at the transition fields that cause damping in the NEMS resonators. In this context, atomistic simulations of MnPS_3 can provide insights into the domain wall dynamics and potentially identify the cause of the transition observed at $\pm 7 \text{ T}$.

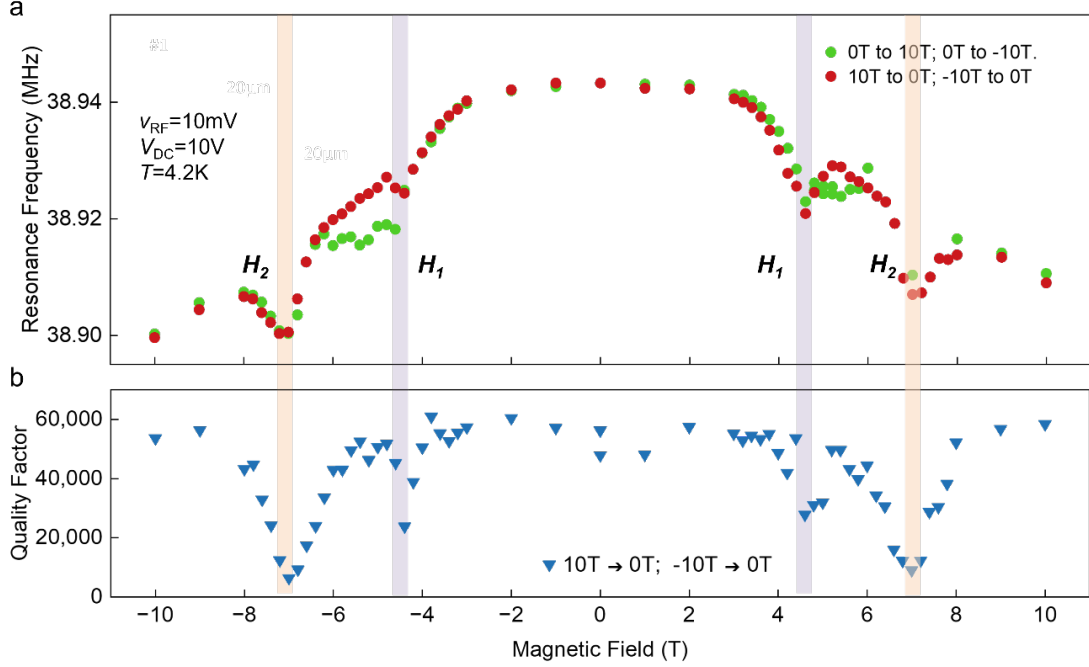


Figure 5: Magnetic field dependence of mechanical resonator in the linear region. (a) Evolution of resonance frequency as a function of the out-of-plane magnetic field measured between ± 10 T. A complete cycle is achieved by sequentially adjusting the magnetic field μH from 0 T to 10 T, then decreased from 10 T to -10 T and finally returned to 0 T. Sharp transitions are observed near $\mu H_1 = \pm 4.6$ T and $\mu H_2 = \pm 7$ T, as indicated by the purple and orange stripes. (b) measured Q factor versus magnetic field shows strong dissipation at the sharp transitions. (Figure obtained from Dr Xiao-Xiao Zhang's group (University of Florida, USA), pending submission)

2 Progress to Date

2.1 Methods

Atomistic simulations were performed using the VAMPIRE software [50] to calculate the magnetic properties of MnPS_3 . The system was described using the spin Hamiltonian:

$$\mathcal{H} = -\frac{1}{2} \sum_{i \neq j} J_{ij} \mathbf{S}_i \cdot \mathbf{S}_j - \frac{1}{2} B \sum_{\text{NN}; i \neq j} (\mathbf{S}_i \cdot \mathbf{S}_j)^2 - K \sum_i (S_i^z)^2 \quad (1)$$

where $\mathbf{S}_{i,j}$ are unit vectors representing the local spin directions on sites i, j . The first term represents bilinear exchange with the exchange constant J_{ij} between spins i and j . The bilinear exchange was considered up to the third nearest neighbour for in-plane and out-of-plane neighbours. The second term describes the biquadratic exchange contribution between site i and its in-plane nearest neighbours and B is the biquadratic exchange constant. Both the bilinear and biquadratic interactions are isotropic. The last term is the easy-axis anisotropy contribution with the magnetocrystalline constant K . Table 1 gives the exchange parameters used for the calculations and Figure 6 shows the different

interactions considered in the calculations.

Parameter	Energy (meV)	Reference
J_1	-7.89	[47]
J_2	-0.21	[47]
J_3	-3.47	[47]
J_4	-0.269	[46]
J_5	-0.107	[46]
J_6	-0.0538	[46]
B	0.95	[47]
K	0.025	[47]

Table 1: In-plane bilinear exchange constants $J_{1,2,3}$ up to third nearest neighbour, out-of-plane bilinear exchange constants $J_{4,5,6}$ up to third nearest neighbour, biquadratic exchange constant B and easy-axis anisotropy constant K for MnPS₃. In-plane exchange couplings J_1-J_3 , B and K were taken from [47] and interlayer exchange couplings J_4-J_6 were taken from [46]

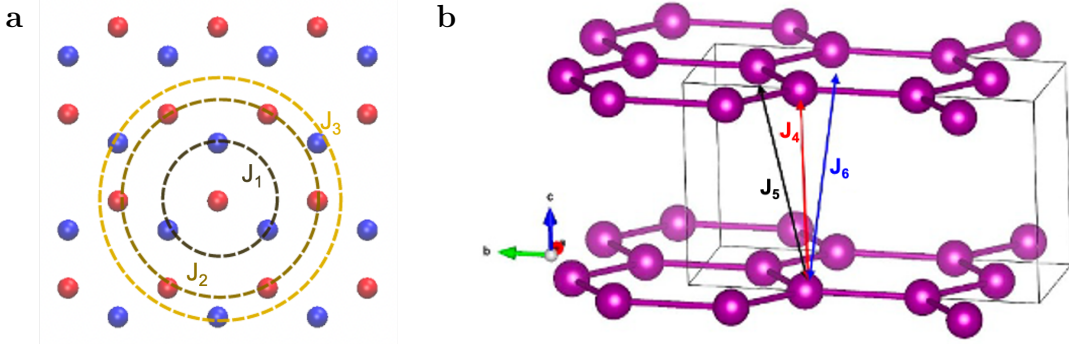


Figure 6: Exchange interactions considered for VAMPIRE simulations of MnPS₃. (a) In-plane (adapted from Ref [45]) (b) out-of-plane (adapted from Ref [46]).

Spin-dynamics simulations were undertaken to determine the stability and motion of domain walls in MnPS₃ ribbons of dimensions 200 nm × 50 nm with 1-7 layers. The simulations were performed by solving the Landau-Lifshitz-Gilbert (LLG) equation:

$$\frac{\partial \mathbf{S}_i}{\partial t} = -\frac{\gamma_e}{1+\alpha^2} [\mathbf{S}_i \times \mathbf{B}_{\text{eff}} + \alpha \mathbf{S}_i \times (\mathbf{S}_i \times \mathbf{B}_{\text{eff}})] \quad (2)$$

which models the interaction of an atomic spin moment \mathbf{S}_i with an effective magnetic field $\mathbf{B}_{\text{eff}} = -\frac{1}{\mu_s} \partial \mathcal{H} / \partial \mathbf{S}_i$. A modified Heun integration method was utilised to increase simulation times up to several nanoseconds. A time step of 0.1 fs, a Gilbert damping parameter $\alpha = 0.01$ [45] and a magnetic moment $\mu_b = 4.68$ [47] for the Mn atoms were used in all simulations. To study domain wall motion, a domain wall was artificially created in the input files and stabilised by field cooling from 0.01 K to 0 K over 0.2 ns, and then the simulation was continued up to 0.4 ns. Then the external magnetic field was applied along the z-axis and the LLG equation was solved to study domain wall dynamics

up to a simulation time of 2 ns. The spin dynamics simulations were carried out at 0 K to isolate the effect of the magnetic field on domain wall motion.

The domain wall velocity was extracted from the motion of the domain wall centre of mass in the same way as Ref. [45]. The atomistic spin configuration of the MnPS₃ ribbon was stored at time intervals of 0.01 ns. At each time interval, the domain wall width and position of the centre of mass were calculated by fitting the z-component of spin, m_z , with the function:

$$m_z(x) = \tanh\left(\frac{x - x_0}{\Delta}\right) \quad (3)$$

where x_0 is the centre of mass of the domain wall and Δ is the Bloch parameter related to domain wall width [51, 52]. The data was fit for the spin chain at the centre of the ribbon to reduce edge effects on the fitting. At each interval, the values of x_0 and Δ were taken from the fit data of the previous interval. The domain wall velocity was then calculated by differentiating the position of the centre of mass with time. An example of the domain wall fitting for 5-layer MnPS₃ at 2 T is shown in Figure 9a.

2.2 Results

2.2.1 Verification of simulation parameters

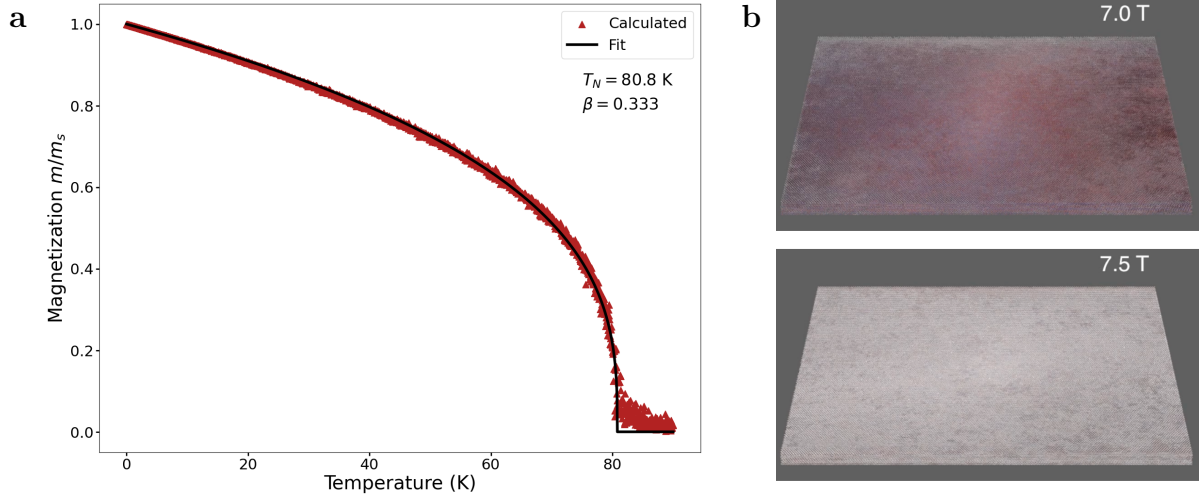


Figure 7: (a) Magnetisation versus temperature for six-layer MnPS₃ using the parameters specified in Table 1. (b) Snapshots of six-layer MnPS₃ at 7 T (top) and 7.5 T (bottom) respectively at a temperature of 4 K. The snapshots show that the spin-flop field in our simulations is higher than experimentally observed values.

To verify the choice of exchange coupling constants, magnetisation as a function of temperature for six-layer MnPS₃ was studied. As shown in Figure 7a we obtain $T_N = 80.8$ K which is in good agreement with the literature values of 78 K [41]. We performed a partial hysteresis simulation from 0 - 10 T to determine the spin-flop field and observed that the spin-flop transition for our parameters takes place between 7 - 7.5 T (Figure 7b). While this does not match experimentally observed values, the small size of the flake (100

$\text{nm} \times 100 \text{ nm}$) in the simulation could introduce finite-size effects that cause an increase in the spin-flop transition field.

2.2.2 Domain wall dynamics of odd-layered MnPS_3

Previous atomistic simulations of MnPS_3 have suggested that anti-ferromagnetic domains may not be intrinsically stable [45] which means that stabilising a domain wall by field cooling from beyond the Néel temperature may not be a feasible method to study domain wall dynamics. In such scenarios, it is helpful to stabilise domain walls by artificially creating a domain wall and field cooling from 0.01 K. We consider MnPS_3 ribbons with 1-7 layers that are 200 nm along a and 49.7 nm along b . Taking into account the edge terminations for field-induced motion from a previous work [45], we have a zig-zag edge on the bottom ($y = 0 \text{ nm}$) and a dangling bond edge on the top ($y = 49.7 \text{ nm}$). Figure 8 shows the stabilised domain wall after 1 ns.

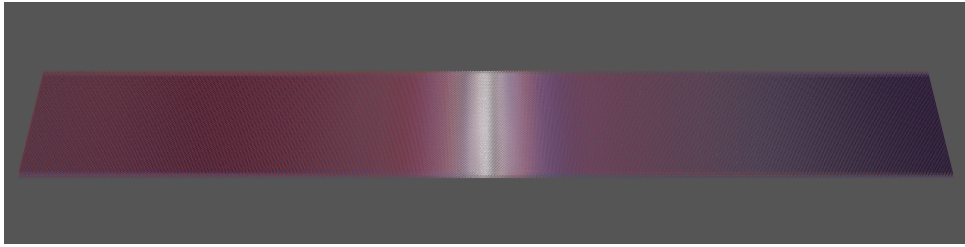


Figure 8: Artificially stabilised domain wall in trilayer MnPS_3 after a simulation time of 1 ns at a temperature of 0 K. Only the z -components of spin are visualised in the snapshot.

After stabilising the domain wall, we apply an out-of-plane magnetic field to the system to study the domain wall dynamics. We consider various fields from 0.2 T to 8 T - beyond the spin-flop field. The domain wall fitting is shown for fields below (2 T), at (7.4 T), and beyond (8 T) the spin-flop field in Figure 9. Below the spin-flop field, the domain wall fitting is straightforward as the spins are primarily aligned along z as shown in the inset in Figure 9a. However, near the spin-flop field, spin waves are emitted in x and y as shown in Figure 10b. This makes the fitting more difficult as the in-plane components of the spin start to dominate. Figure 9b shows the fitting for 5-layer MnPS_3 at a field of 7.4 T, close to the spin-flop field in our simulations. The fitting quality is slightly reduced as m_z no longer goes from 1 to -1 but is still accurate enough to extract the domain wall velocity. Beyond the spin-flop transition field, the in-plane components of spin dominate and Eq 3 can no longer be used to fit the data for 8 T as shown in Figure 9c. As a result, domain wall velocities are only extracted up to 7.8 T which is just beyond the spin-flop transition field for our simulations.

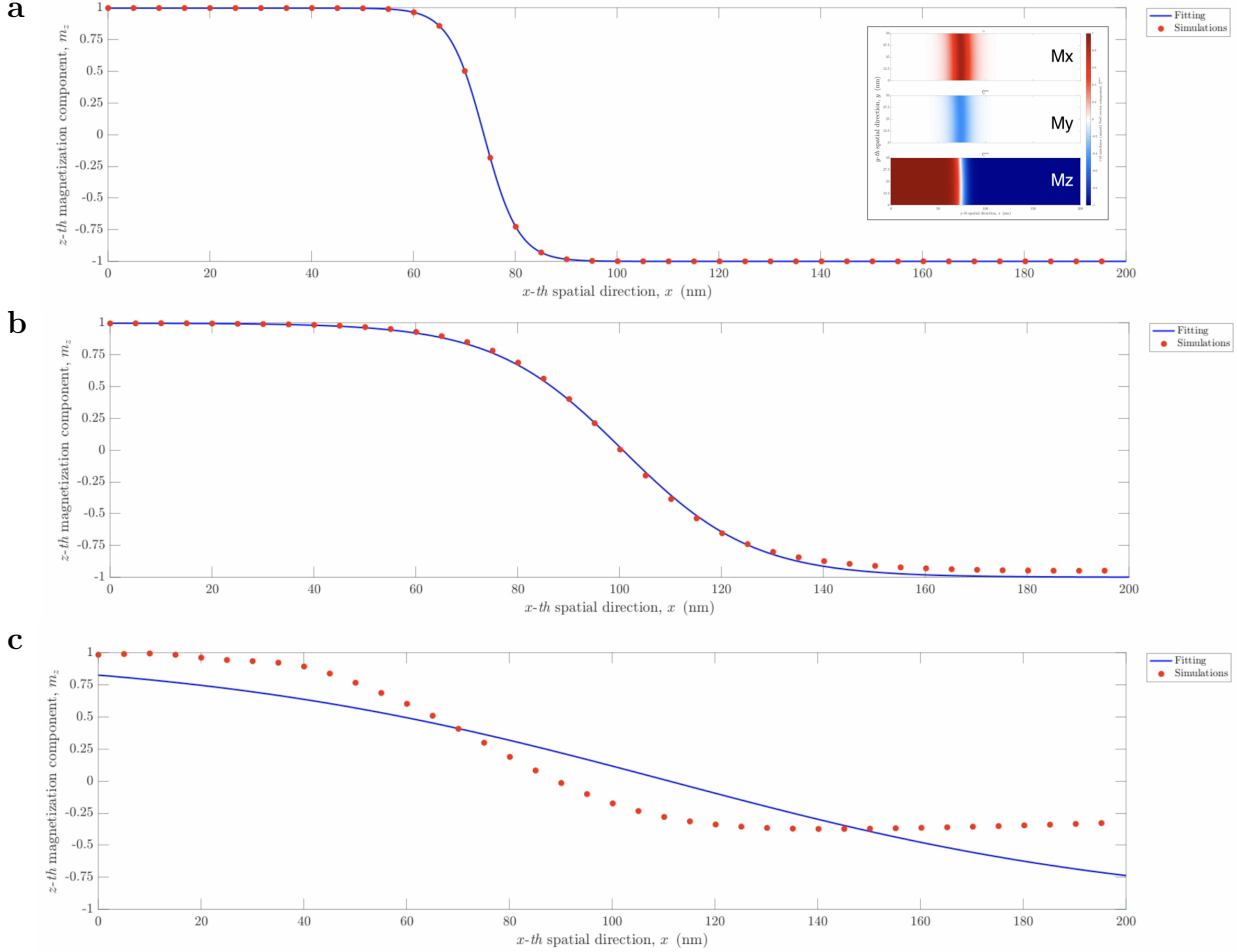


Figure 9: Domain wall fitting for 5-layer MnPS_3 with an external field of (a) 2 T, (b) 7.4 T and (c) 8T. The m_z data is fit to Eq. 3 for the middle spin-chain ($y \sim 25 \text{ nm}$) of the MnPS_3 ribbon. Inset in (a) shows the x (top), y (middle) and z (bottom) spin components of the MnPS_3 ribbon at 2 T. The temperature is 0 K.

For the case of odd-layered MnPS_3 , we observe domain wall motion that can be attributed to the interaction of the uncompensated layer with the magnetic field. At low fields, the spins are primarily oriented along z and the in-plane components of spin are not very pronounced. As the field is increased, the domain wall speed increases and we also observe a bending of the domain wall due to faster propagation along the dangling bond edge compared to the zig-zag edge, which can be seen in Figure 10a. As shown in Figure 11a, the domain wall speeds peak at the spin-flop field and remain fairly constant with increasing field. Additionally, the emission of spin waves in x and y can be observed (Figure 10b) at these fields. The spin waves could act as a dissipation channel and lead to the loss of the Q factor observed in Figure 5b.

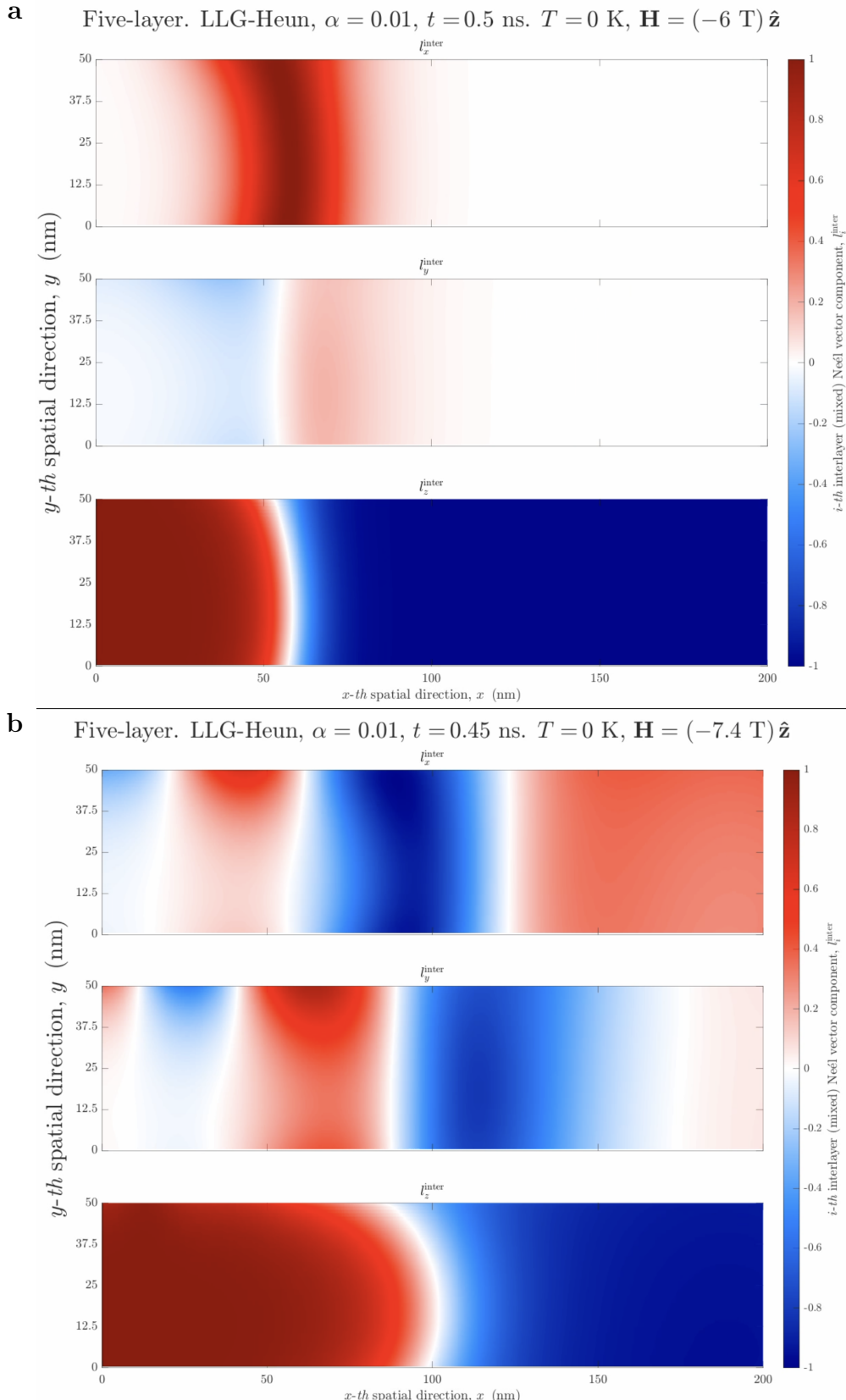


Figure 10: x , y and z components of spin of five-layer MnPS_3 ribbon at a field of (a) 6 T, (b) 7.4 T. Domain wall widening can be observed in (a) as the x component grows larger. Spin waves in x and y directions can clearly be seen in (b).

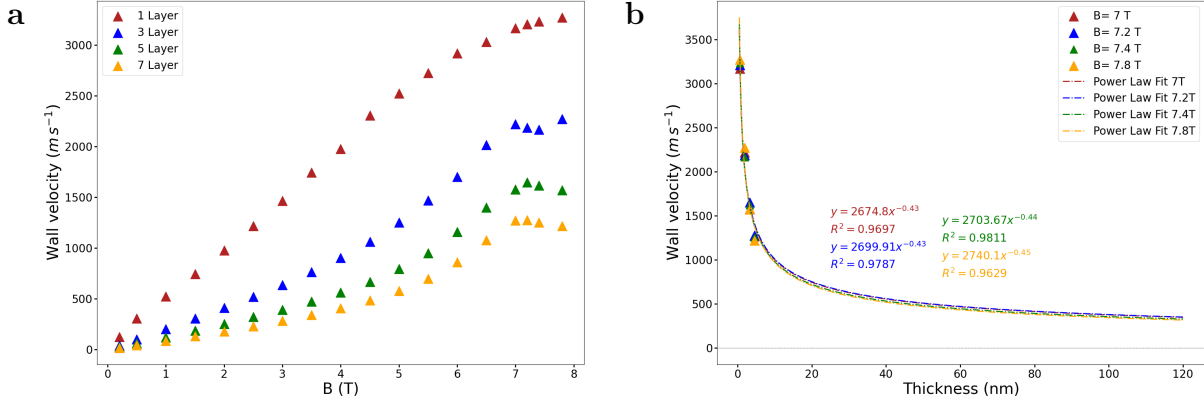


Figure 11: (a) Calculated domain wall velocity from simulations. (b) Thickness dependence of domain wall velocity

We also see a thickness dependence of the domain wall velocity for a constant field, shown in Figure 11b. As we increase the number of layers, the effect of the uncompensated layer reduces and so the velocity of the domain wall reduces. However, upon extrapolating the trends for fields near the spin-flop transition, we can see that the domain walls have a velocity of 450 m/s even at a thickness of 100 nm. The high speeds at the spin-flop fields suggest that there may be some fast dynamics of the in-plane spins beyond the spin-flop transition that could be related to the transition observed at higher fields.

2.2.3 Domain wall dynamics of even-layered MnPS_3

In the case of even layers, the domain walls remain "pinned" as all the layers are compensated. With increasing field, we observe a gradual increase in domain wall width but no motion of the walls. Even at fields as high as 6 T, there is no motion of domain walls after 2 ns, as depicted in Figure 12a. As we approach the spin-flop transition, there are spin waves emitted in the x and y directions similar to the odd-layered case. Interestingly, even though spin waves are emitted in both cases, the in-plane components are larger than the z component for the even-layered case compared to the odd layers. This could be due to the spins being compensated in the even-layered case resulting in no net magnetisation along z as opposed to the odd layers. The exchange interactions thus force the spins to an in-plane configuration more rapidly in the even-layered case than in the odd-layered case.

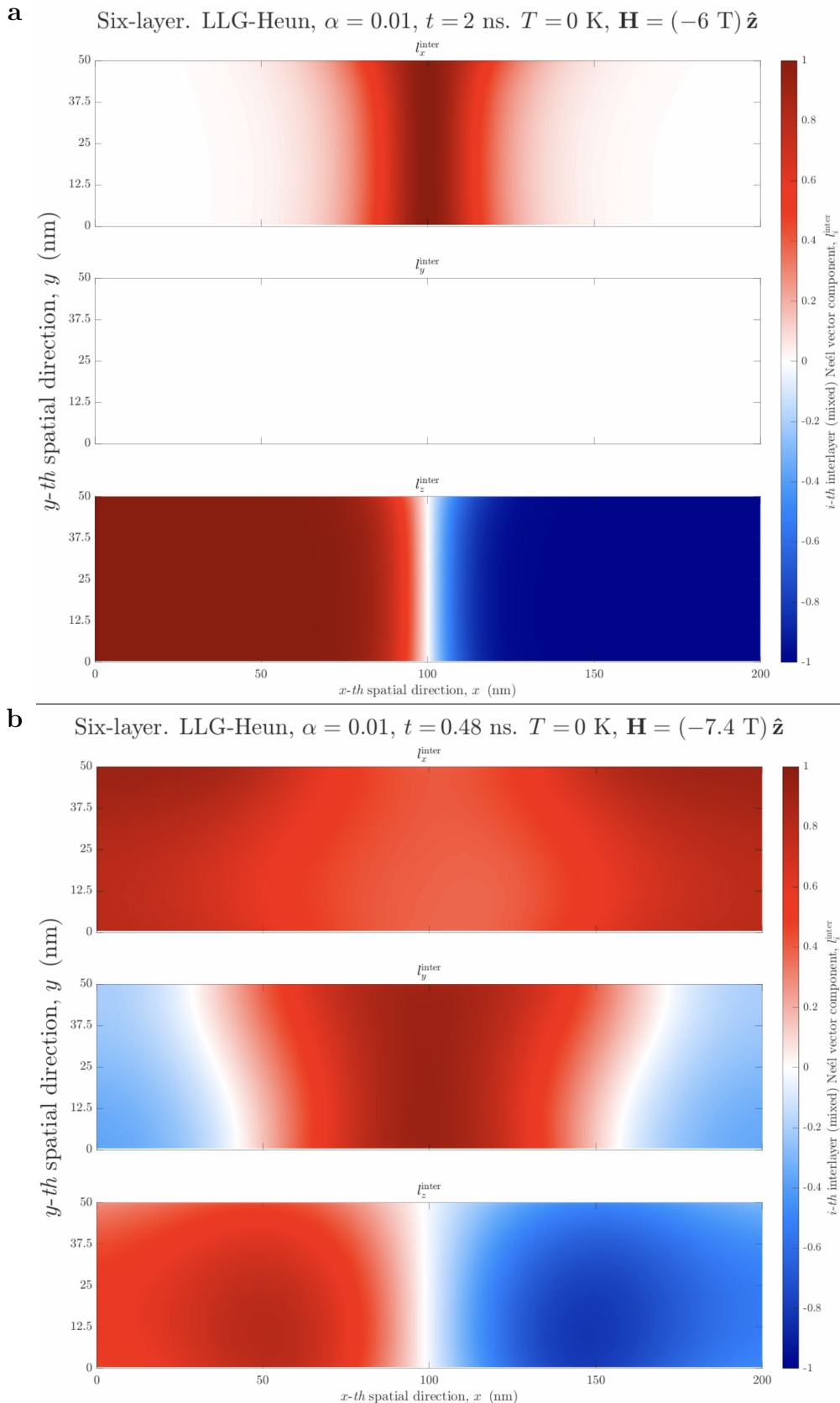


Figure 12: x , y and z components of spin of six-layer MnPS_3 ribbon at a field of (a) 6 T, (b) 7.4 T. Domain wall widening can be observed in (a) as the x and y component grows larger. Spin waves in x and y directions can clearly be seen in (b).

3 Future Work

A large portion of the current work has focused on the domain wall dynamics of few-layered MnPS_3 with results that provide insights into the microscopic behaviour of magnetic transitions. While these results offer some backbone to the hypotheses and data put forth by Dr Zhang and her group, the exact mechanisms of the second transition at ± 7 T are yet to be understood. Future studies will focus on the underlying mechanism of the second transition and whether it is controlled by domain wall dynamics or magnetoelastic interactions that are known to persist even beyond the Néel temperature [46].

Furthermore, MnPS_3 is only a single member of the widely studied MPX_3 family. Other members like FePS_3 and NiPS_3 are yet to be the focus of theoretical approaches to studying magnetic behaviour. FePS_3 and NiPS_3 have higher Néel temperatures than MnPS_3 and as such are already lucrative options for devices [41]. The atomistic methods used in the current work will be applied to other materials of the MPX_3 family. The exchange parameters for FePS_3 and NiPS_3 are already available in existing literature [47] and are ready to use. The presence of DMI in FePS_3 could be vital to stabilising topological spin textures such as skyrmions, which will be one of the focuses of future work. Additionally, Dr Zhang will also be exploring the magnetic properties of NiPS_3 in which neighbouring zig-zag chains are anti-ferromagnetically coupled [40]. This coupling between the chains could lead to more dominant spin-wave behaviour and future work will aim to study this possibility and continue the collaboration between Dr Zhang's research group and our own.

Finally, 2D magnetic materials such as Fe_3GeTe_2 and Fe_3GaTe_2 are promising for next-generation devices as they have Curie temperatures that are close to room temperature [53]. During the following year, my research will focus on understanding the magnetic properties of these room-temperature 2D magnets. Their applicability to devices relies on magnetic switching and so future research will focus on the behaviour of these materials in response to external electric or magnetic fields.

4 Summary

Motivated by the growing energy concerns, the next generation of devices requires rapid development in their energy efficiency. Among the various applications, anti-ferromagnetic spintronics stands out in particular as an emerging field due to the robust protection of magnetic data and fast dynamics that anti-ferromagnets offer. With the recent exploration in 2D magnetism, layered vdW materials such as the MPX_3 family are an appealing choice due to the wide array of magnetic properties they show [41, 40]. The key members of the family MnPS_3 , NiPS_3 and FePS_3 can be described by the Heisenberg, XY and Ising models respectively, proving the versatility of these compounds. In particular, MnPS_3 has a Néel anti-ferromagnetic ground state [41] and studies have shown fully switchable magnon transport [44]. Past work has demonstrated the sensitivity of monolayer MnPS_3 to electric and magnetic fields with the help of atomistic simulations [45]. This work is part of an ongoing collaboration wherein NEMS resonators have been used to detect two magnetic transitions in MnPS_3 at ± 4.6 T and ± 7 T. The ± 4.6 T transition is attributed to the spin-flop transition [49]. Atomistic simulations of MnPS_3 were performed to study domain wall dynamics and gain insights into the high-field transition. Domain

wall motion was observed for odd-layered flakes due to uncompensated spins in the top layer interacting with the applied magnetic field. The domain wall velocities increased with the field and as the fields approached the spin-flop field, domain wall bending was observed. At the spin-flop field and beyond, the velocities were more or less constant but the distribution of the spins revealed spin waves being emitted in x and y directions. Additionally, the domain wall velocities decreased with thickness for a given field. However, even at thicknesses of 100 nm, the speeds were 450 m/s implying that the spin-flop state could have various in-plane fast dynamics that can contribute to the ± 7 T transition. In the even-layered flakes, the domain wall remained pinned up till the spin-flop field with only an increase in domain wall width. Beyond the spin-flop field, spin waves were again emitted in x and y although the in-plane components quickly overcame the z component of spin, unlike the odd-layered case where the z component remained dominant. With the immense scope of 2D anti-ferromagnets for spintronics applications, it is important to combine experiments with theory to gain a complete understanding of the magnetic behaviour of these materials. This work, and future projects, will aim to apply these methods to other interesting 2D anti-ferromagnets, especially those of the MPX₃ family such as FePS₃ and NiPS₃ whose higher Néel temperatures make them promising candidates for next-generation energy-efficient devices.

References

- [1] The Paris Agreement | UNFCCC.
- [2] United Nations. Net Zero Coalition. Publisher: United Nations.
- [3] Gordon E. Moore. Cramming more components onto integrated circuits, Reprinted from Electronics, volume 38, number 8, April 19, 1965, pp.114 ff. *IEEE Solid-State Circuits Society Newsletter*, 11(3):33–35, September 2006. Conference Name: IEEE Solid-State Circuits Society Newsletter.
- [4] Gordon E. Moore. Progress in digital integrated electronics [Technical literature, Copyright 1975 IEEE. Reprinted, with permission. Technical Digest. International Electron Devices Meeting, IEEE, 1975, pp. 11-13.]. *IEEE Solid-State Circuits Society Newsletter*, 11(3):36–37, September 2006. Conference Name: IEEE Solid-State Circuits Society Newsletter.
- [5] Thomas N. Theis and H.-S. Philip Wong. The End of Moore’s Law: A New Beginning for Information Technology. *Computing in Science & Engineering*, 19(2):41–50, March 2017. Conference Name: Computing in Science & Engineering.
- [6] Mark Lundstrom. Moore’s Law Forever? *Science*, 299(5604):210–211, January 2003. Publisher: American Association for the Advancement of Science.
- [7] Charbel Tannous and R. Lawrence Comstock. Magnetic Information-Storage Materials. In *Springer Handbook of Electronic and Photonic Materials*. Springer Cham, January 2017.
- [8] Sabpreet Bhatti, Rachid Sbiaa, Atsufumi Hirohata, Hideo Ohno, Shunsuke Fukami, and S. N. Piramanayagam. Spintronics based random access memory: a review. *Materials Today*, 20(9):530–548, November 2017.

- [9] K. S. Novoselov, A. K. Geim, S. V. Morozov, D. Jiang, Y. Zhang, S. V. Dubonos, I. V. Grigorieva, and A. A. Firsov. Electric Field Effect in Atomically Thin Carbon Films. *Science*, 306(5696):666–669, October 2004. Publisher: American Association for the Advancement of Science.
- [10] Ankur Gupta, Tamilselvan Sakthivel, and Sudipta Seal. Recent development in 2D materials beyond graphene. *Progress in Materials Science*, 73:44–126, August 2015.
- [11] Xiaoyan Zhang, Lili Hou, Artur Ciesielski, and Paolo Samorì. 2D Materials Beyond Graphene for High-Performance Energy Storage Applications. *Advanced Energy Materials*, 6(23):1600671, 2016. eprint: <https://onlinelibrary.wiley.com/doi/pdf/10.1002/aenm.201600671>.
- [12] Vigneshwaran Shanmugam, Rhoda Afriyie Mensah, Karthik Babu, Sidique Gawusu, Avishek Chanda, Yongming Tu, Rasoul Esmaeely Neisiany, Michael Försth, Gabriel Sas, and Oisik Das. A Review of the Synthesis, Properties, and Applications of 2D Materials. *Particle & Particle Systems Characterization*, 39(6):2200031, 2022. eprint: <https://onlinelibrary.wiley.com/doi/pdf/10.1002/ppsc.202200031>.
- [13] Shreyas Ramachandran, K. V. Sai Srinivasan, and Ravindran Sujith. Nickel-decorated single vacancy phosphorene – A favourable candidate for hydrogen storage. *International Journal of Hydrogen Energy*, 46(54):27597–27611, August 2021.
- [14] Sai Srinivasan K V, Aqshat Seth, Dhammapada Mohapatra, Shreyas Ramachandran, and Ravindran Sujith. Iron decorated defective phosphorene as a viable hydrogen storage medium – A DFT study. *International Journal of Hydrogen Energy*, 47(82):34976–34993, September 2022.
- [15] N. D. Mermin and H. Wagner. Absence of Ferromagnetism or Antiferromagnetism in One- or Two-Dimensional Isotropic Heisenberg Models. *Physical Review Letters*, 17(22):1133–1136, November 1966. Publisher: American Physical Society.
- [16] Cheng Gong, Lin Li, Zhenglu Li, Huiwen Ji, Alex Stern, Yang Xia, Ting Cao, Wei Bao, Chenzhe Wang, Yuan Wang, Z. Q. Qiu, R. J. Cava, Steven G. Louie, Jing Xia, and Xiang Zhang. Discovery of intrinsic ferromagnetism in two-dimensional van der Waals crystals. *Nature*, 546(7657):265–269, June 2017. Publisher: Nature Publishing Group.
- [17] Bevin Huang, Genevieve Clark, Efrén Navarro-Moratalla, Dahlia R. Klein, Ran Cheng, Kyle L. Seyler, Ding Zhong, Emma Schmidgall, Michael A. McGuire, David H. Cobden, Wang Yao, Di Xiao, Pablo Jarillo-Herrero, and Xiaodong Xu. Layer-dependent ferromagnetism in a van der Waals crystal down to the monolayer limit. *Nature*, 546(7657):270–273, June 2017. Publisher: Nature Publishing Group.
- [18] Qing Hua Wang, Amilcar Bedoya-Pinto, Mark Blei, Avalon H. Dismukes, Assaf Hamo, Sarah Jenkins, Maciej Koperski, Yu Liu, Qi-Chao Sun, Evan J. Telford, Hyun Ho Kim, Mathias Augustin, Uri Vool, Jia-Xin Yin, Lu Hua Li, Alexey Falin, Cory R. Dean, Fèlix Casanova, Richard F. L. Evans, Mairbek Chshiev, Artem Mishchenko, Cedomir Petrovic, Rui He, Liuyan Zhao, Adam W. Tsien, Brian D. Gerardot, Mauro Brotons-Gisbert, Zurab Guguchia, Xavier Roy, Sefaattin Tongay, Ziwei Wang, M. Zahid Hasan, Joerg Wrachtrup, Amir Yacoby, Albert Fert, Stuart

- Parkin, Kostya S. Novoselov, Pengcheng Dai, Luis Balicas, and Elton J. G. Santos. The Magnetic Genome of Two-Dimensional van der Waals Materials. *ACS Nano*, 16(5):6960–7079, May 2022. Publisher: American Chemical Society.
- [19] Sarah Jenkins, Levente Rózsa, Unai Atxitia, Richard F. L. Evans, Kostya S. Novoselov, and Elton J. G. Santos. Breaking through the Mermin-Wagner limit in 2D van der Waals magnets. *Nature Communications*, 13(1):6917, November 2022. Number: 1 Publisher: Nature Publishing Group.
- [20] Wei Han, Roland K. Kawakami, Martin Gmitra, and Jaroslav Fabian. Graphene spintronics. *Nature Nanotechnology*, 9(10):794–807, October 2014. Publisher: Nature Publishing Group.
- [21] Michael A. McGuire, Hemant Dixit, Valentino R. Cooper, and Brian C. Sales. Coupling of Crystal Structure and Magnetism in the Layered, Ferromagnetic Insulator CrI₃. *Chemistry of Materials*, 27(2):612–620, January 2015. Publisher: American Chemical Society.
- [22] Zaiyao Fei, Bevin Huang, Paul Malinowski, Wenbo Wang, Tiancheng Song, Joshua Sanchez, Wang Yao, Di Xiao, Xiaoyang Zhu, Andrew F. May, Weida Wu, David H. Cobden, Jiun-Haw Chu, and Xiaodong Xu. Two-dimensional itinerant ferromagnetism in atomically thin Fe₃GeTe₂. *Nature Materials*, 17(9):778–782, September 2018. Publisher: Nature Publishing Group.
- [23] Cheng-Tai Kuo, Michael Neumann, Karuppannan Balamurugan, Hyun Ju Park, Soonmin Kang, Hung Wei Shiu, Jin Hyoun Kang, Byung Hee Hong, Moonsup Han, Tae Won Noh, and Je-Geun Park. Exfoliation and Raman Spectroscopic Fingerprint of Few-Layer NiPS₃ Van der Waals Crystals. *Scientific Reports*, 6(1):20904, February 2016. Publisher: Nature Publishing Group.
- [24] Michael A. McGuire, Genevieve Clark, Santosh KC, W. Michael Chance, Gerald E. Jellison, Valentino R. Cooper, Xiaodong Xu, and Brian C. Sales. Magnetic behavior and spin-lattice coupling in cleavable van der Waals layered $\{\text{CrCl}\}_3$ crystals. *Physical Review Materials*, 1(1):014001, June 2017. Publisher: American Physical Society.
- [25] Xiao Wang, Jian Tang, Xiuxin Xia, Congli He, Junwei Zhang, Yizhou Liu, Caihua Wan, Chi Fang, Chenyang Guo, Wenlong Yang, Yao Guang, Xiaomin Zhang, Hongjun Xu, Jinwu Wei, Mengzhou Liao, Xiaobo Lu, Jiafeng Feng, Xiaoxi Li, Yong Peng, Hongxiang Wei, Rong Yang, Dongxia Shi, Xixiang Zhang, Zheng Han, Zhidong Zhang, Guangyu Zhang, Guoqiang Yu, and Xiufeng Han. Current-driven magnetization switching in a van der Waals ferromagnet Fe₃GeTe₂. *Science Advances*, 5(8):eaaw8904, August 2019. Publisher: American Association for the Advancement of Science.
- [26] Maya Khela, Maciej Dabrowski, Safe Khan, Paul S. Keatley, Ivan Verzhbitskiy, Goki Eda, Robert J. Hicken, Hidekazu Kurebayashi, and Elton J. G. Santos. Laser-induced topological spin switching in a 2D van der Waals magnet. *Nature Communications*, 14(1):1378, March 2023. Number: 1 Publisher: Nature Publishing Group.

- [27] Tae-Eon Park, Licong Peng, Jinghua Liang, Ali Hallal, Fehmi Sami Yasin, Xichao Zhang, Kyung Mee Song, Sung Jong Kim, Kwangsu Kim, Markus Weigand, Gisela Schütz, Simone Finizio, Jörg Raabe, Karin Garcia, Jing Xia, Yan Zhou, Motohiko Ezawa, Xiaoxi Liu, Joonyeon Chang, Hyun Cheol Koo, Young Duck Kim, Mairbek Chshiev, Albert Fert, Hongxin Yang, Xiuzhen Yu, and Seonghoon Woo. N\'eel-type skyrmions and their current-induced motion in van der Waals ferromagnet-based heterostructures. *Physical Review B*, 103(10):104410, March 2021. Publisher: American Physical Society.
- [28] Mara Strungaru, Mathias Augustin, and Elton J. G. Santos. Ultrafast laser-driven topological spin textures on a 2D magnet. *npj Computational Materials*, 8(1):1–6, August 2022. Number: 1 Publisher: Nature Publishing Group.
- [29] Igor Žutić, Jaroslav Fabian, and S. Das Sarma. Spintronics: Fundamentals and applications. *Reviews of Modern Physics*, 76(2):323–410, April 2004. Publisher: American Physical Society.
- [30] Tiancheng Song, Zaiyao Fei, Matthew Yankowitz, Zhong Lin, Qianni Jiang, Kyle Hwangbo, Qi Zhang, Bosong Sun, Takashi Taniguchi, Kenji Watanabe, Michael A. McGuire, David Graf, Ting Cao, Jiun-Haw Chu, David H. Cobden, Cory R. Dean, Di Xiao, and Xiaodong Xu. Switching 2D magnetic states via pressure tuning of layer stacking. *Nature Materials*, 18(12):1298–1302, December 2019. Publisher: Nature Publishing Group.
- [31] Maciej Dabrowski, Shi Guo, Mara Strungaru, Paul S. Keatley, Freddie Withers, Elton J. G. Santos, and Robert J. Hicken. All-optical control of spin in a 2D van der Waals magnet. *Nature Communications*, 13(1):5976, October 2022. Publisher: Nature Publishing Group.
- [32] Shengwei Jiang, Jie Shan, and Kin Fai Mak. Electric-field switching of two-dimensional van der Waals magnets. *Nature Materials*, 17(5):406–410, May 2018. Publisher: Nature Publishing Group.
- [33] Gaojie Zhang, Qingyuan Luo, Xiaokun Wen, Hao Wu, Li Yang, Wen Jin, Luji Li, Jia Zhang, Wenfeng Zhang, Haibo Shu, and Haixin Chang. Giant 2D Skyrmiion Topological Hall Effect with Ultrawide Temperature Window and Low-Current Manipulation in 2D Room-Temperature Ferromagnetic Crystals. *Chinese Physics Letters*, 40(11):117501, November 2023. Publisher: Chinese Physical Society and IOP Publishing Ltd.
- [34] I. Dzyaloshinsky. A thermodynamic theory of “weak” ferromagnetism of antiferromagnetics. *Journal of Physics and Chemistry of Solids*, 4(4):241–255, January 1958.
- [35] Tōru Moriya. Anisotropic Superexchange Interaction and Weak Ferromagnetism. *Physical Review*, 120(1):91–98, October 1960. Publisher: American Physical Society.
- [36] X. Z. Yu, Y. Onose, N. Kanazawa, J. H. Park, J. H. Han, Y. Matsui, N. Nagaosa, and Y. Tokura. Real-space observation of a two-dimensional skyrmion crystal. *Nature*, 465(7300):901–904, June 2010. Publisher: Nature Publishing Group.

- [37] Daoqian Zhu, Wang Kang, Sai Li, Yangqi Huang, Xichao Zhang, Yan Zhou, and Weisheng Zhao. Skyrmiion Racetrack Memory With Random Information Update/Deletion/Insertion. *IEEE Transactions on Electron Devices*, 65(1):87–95, January 2018. Conference Name: IEEE Transactions on Electron Devices.
- [38] T. Jungwirth, X. Marti, P. Wadley, and J. Wunderlich. Antiferromagnetic spintronics. *Nature Nanotechnology*, 11(3):231–241, March 2016. Publisher: Nature Publishing Group.
- [39] E. V. Gomonay and V. M. Loktev. Spintronics of antiferromagnetic systems (Review Article). *Low Temperature Physics*, 40(1):17–35, January 2014.
- [40] M. J. Coak, D. M. Jarvis, H. Hamidov, C. R. S. Haines, P. L. Alireza, C. Liu, Suhan Son, Inho Hwang, G. I. Lampronti, D. Daisenberger, P. Nahai-Williamson, A. R. Wildes, S. S. Saxena, and Je-Geun Park. Tuning dimensionality in van-der-Waals antiferromagnetic Mott insulators TMPS3. *Journal of Physics: Condensed Matter*, 32(12):124003, December 2019. Publisher: IOP Publishing.
- [41] Fengmei Wang, Tofik A. Shifa, Peng Yu, Peng He, Yang Liu, Feng Wang, Zhenxing Wang, Xueying Zhan, Xiaoding Lou, Fan Xia, and Jun He. New Frontiers on van der Waals Layered Metal Phosphorous Trichalcogenides. *Advanced Functional Materials*, 28(37):1802151, 2018. -eprint: <https://onlinelibrary.wiley.com/doi/pdf/10.1002/adfm.201802151>.
- [42] Wenyu Xing, Luyi Qiu, Xirui Wang, Yunyan Yao, Yang Ma, Ranran Cai, Shuang Jia, X. C. Xie, and Wei Han. Magnon Transport in Quasi-Two-Dimensional van der Waals Antiferromagnets. *Physical Review X*, 9(1):011026, February 2019. Publisher: American Physical Society.
- [43] D. Lançon, R. A. Ewings, T. Guidi, F. Formisano, and A. R. Wildes. Magnetic exchange parameters and anisotropy of the quasi-two-dimensional antiferromagnet \$\mathrm{NiPS}_3\$. *Physical Review B*, 98(13):134414, October 2018. Publisher: American Physical Society.
- [44] Guangyi Chen, Shaomian Qi, Jianqiao Liu, Di Chen, Jiongjie Wang, Shili Yan, Yu Zhang, Shimin Cao, Ming Lu, Shibing Tian, Kangyao Chen, Peng Yu, Zheng Liu, X. C. Xie, Jiang Xiao, Ryuichi Shindou, and Jian-Hao Chen. Electrically switchable van der Waals magnon valves. *Nature Communications*, 12(1):6279, November 2021. Number: 1 Publisher: Nature Publishing Group.
- [45] Ignacio M. Alliati, Richard F. L. Evans, Kostya S. Novoselov, and Elton J. G. Santos. Relativistic domain-wall dynamics in van der Waals antiferromagnet MnPS3. *npj Computational Materials*, 8(1):1–9, January 2022. Number: 1 Publisher: Nature Publishing Group.
- [46] Diana Vaclavkova, Alex Delhomme, Clément Faugeras, Marek Potemski, Aleksander Bogucki, Jan Suffczyński, Piotr Kossacki, Andrew R. Wildes, Benoit Grémaud, and Andrés Saúl. Magnetoelastic interaction in the two-dimensional magnetic material MnPS3 studied by first principles calculations and Raman experiments. *2D Materials*, 7(3):035030, June 2020. Publisher: IOP Publishing.

- [47] M. Amirabbasi and P. Kratzer. Effect of biquadratic magnetic exchange interaction in the 2D antiferromagnets $M\{\mathrm{PS}\}_3$ ($M=\mathrm{Mn}, \mathrm{Fe}, \mathrm{Co}, \mathrm{Ni}$). *Physical Review Materials*, 8(8):084005, August 2024. Publisher: American Physical Society.
- [48] Miłosz Rybak, Paulo E. Faria Junior, Tomasz Woźniak, Paweł Scharoch, Jaroslav Fabian, and Magdalena Birowska. Magneto-optical anisotropies of two-dimensional antiferromagnetic $M\{\mathrm{P}\}\{\mathrm{X}\}_3$ from first principles. *Physical Review B*, 109(5):054426, February 2024. Publisher: American Physical Society.
- [49] Gen Long, Hugo Henck, Marco Gibertini, Dumitru Dumcenco, Zhe Wang, Takashi Taniguchi, Kenji Watanabe, Enrico Giannini, and Alberto F. Morpurgo. Persistence of Magnetism in Atomically Thin MnPS₃ Crystals. *Nano Letters*, 20(4):2452–2459, April 2020. Publisher: American Chemical Society.
- [50] R. F. L. Evans, W. J. Fan, P. Chureemart, T. A. Ostler, M. O. A. Ellis, and R. W. Chantrell. Atomistic spin model simulations of magnetic nanomaterials. *Journal of Physics: Condensed Matter*, 26(10):103202, February 2014. Publisher: IOP Publishing.
- [51] N. L. Schryer and L. R. Walker. The motion of 180° domain walls in uniform dc magnetic fields. *Journal of Applied Physics*, 45(12):5406–5421, December 1974.
- [52] R. Rama-Eiroa, P. E. Roy, J. M. González, K. Y. Guslienko, J. Wunderlich, and R. M. Otxoa. Inertial domain wall characterization in layered multisublattice antiferromagnets. *Journal of Magnetism and Magnetic Materials*, 560:169566, October 2022.
- [53] Xia Chen, Xi Zhang, and Gang Xiang. Recent advances in two-dimensional intrinsic ferromagnetic materials Fe 3 X (X =Ge and Ga)Te 2 and their heterostructures for spintronics. *Nanoscale*, 16(2):527–554, 2024. Publisher: Royal Society of Chemistry.